Supplementary Information

Engineering Pt nanoclusters on CeO_2 surface with abundant point defects by in situ confined-domain encapsulation strategy for the catalytic elimination of VOCs

Siyi Ma[a,b], Fang Dong[a,c], Weiliang Han[a], Weigao Han[a], Zhicheng Tang[a*]

(a. National Engineering Research Center for Fine Petrochemical Intermediates, and State Key Laboratory for Oxo Synthesis and Selective Oxidation, Lanzhou Institute of Chemical Physics, Chinese Academy of Sciences, Lanzhou 730000, China)

(b. University of Chinese Academy of Sciences, Beijing 100039, China)

(c. Dalian National Laboratory for Clean Energy, Dalian Institute of Chemical Physics, Chinese Academy of Sciences, Dalian, 116023, China)

*Corresponding author.

Tel.: +86-931-4968083, E-mail address: tangzhicheng@licp.cas.cn (Z. Tang).

1. Experimental section

1.1 Preparation of $Pt_{NP}@CeO_2$ (n-$NaBH_4$) sample

3.472 g $Ce(NO_3)_3 \cdot 6H_2O$ and a small amount of PVA (PVA/noble metal mass ratio = 1.2:1.0) were dissolved in 20 mL of deionized water (90 °C). After cooling, a quantity of H_2PtCl_6 (0.037 mL) was added to form solution A. 18 g of NaOH (6 mol/L) was diluted in 140 mL deionized water to become solution B, and then the solution B was added to solution A to create solution C. The subsequent operation was consistent with the preparation of $Pt_{NP}@CeO_2$. The prepared sample was labeled as $Pt_{NP}@CeO_2$ (n-$NaBH_4$).

1.2 Characterization technique

The morphology of the catalyst samples was analyzed by transmission electron microscopy (TEM, JEOL-JEM-2010). The crystal phases of each element in the catalyst were determined by X-ray diffraction instrument (XRD, Japan Smartlabse) (scanning angle of 10°-90°, scanning speed of 0.5 °/min, 60 kV, 55 mA) under the radiation of λ=1.5406 nm. The Fourier transform infrared spectroscopy (FTIR) analysis of the samples was performed using Fourier infrared spectrometer (Nexus 870, Nicolet), and ATR technology was used for FTIR analysis. The Raman spectroscopy test was performed on the LabramHR Evolution Raman spectrometer with a 532 nm laser source and a scanning range of 100 to 1,200 cm^{-1}. Brunauer-emmett-teller (BET) surface area, the pore size and pore volume of the catalysts was obtained by adsorption and desorption of nitrogen in ASAP 2020 instrument (America Micromeritics). The real content of each metal on the catalyst was obtained

by measuring each catalyst with an Agilent ICP-OES 730 instrument. Infrared spectra were tested with a Nicolet Nexus 870 Fourier transform infrared spectrometer. X-ray photoelectron spectroscopy (XPS) measurements were performed with a Thermo Scientific 250 Xi.

The multifunctional dynamic adsorption instrument TP-5080-D was used to analyze the acidity and redox capacity of the catalyst surface. For H_2-TPR, a 50 mg sample was heated from room temperature to 900 ^oC in reduced gas with volume fractions of 5 vol % H_2 and 95 vol % N_2, and the detector signal was continuously recorded. For the O_2-TPD test, the catalyst (50 mg) was pretreated with nitrogen (99.9%) for 1 h at 300 ^oC. When the temperature dropped to 50 ^oC, the O_2 adsorption was carried out for 60 min. After the adsorption was over, purged with pure He for 0.5 h, and the desorbed O_2 signal was detected at 50-900 ^oC. The temperature-programmed desorption operation of NH_3-TPD was similar to that of O_2-TPD, except that O_2 was changed to NH_3.

1.3 Performance measurement

Tests of activity and stability were essential for probing catalytic performance, mainly with the help of fixed-bed reactor. By pressing and sieving (40-60 mesh), it was possible to obtain 0.4 g of sample, to which 0.7 g of silica (SiO_2) was subsequently added. The catalyst and SiO_2 were mixed well and poured into the thermostatic zone of the reaction tube, which was stuffed with cotton. The catalyst was exposed to a mixture of toluene (3000 ppm) and air with a flow rate of 200 mL/min and a weight hourly space velocity (WHSV) of 30 000 $mL \cdot g^{-1} \cdot h^{-1}$. An on-line

gas chromatograph (GC-6820, Agilent, USA) equipped with a flame ionization detector (FID) was used to detect the concentration of the reactants. Usually, the activity was distinguished by the reaction temperature when the toluene conversion was 90%. The toluene conversion was calculated as follows:

$$Conversion\ of\ toluene = \frac{Toluene_{in} - Toluene_{out}}{Toluene_{in}} \times 100\%$$

Generally, to test the stability of the catalyst, it is necessary to keep the reaction temperatures at high/low conversion of toluene for about 15 hours. And the concentration of the reactants was measured every hour to calculate the toluene conversion. In general, the specific equation for carbon balance was as follows and the error of carbon balance is about ±3%:

$$Carbon\ balance\ (\%) = \frac{Mole\ of\ the\ overall\ carbon\ fed\ (mol)}{Mole\ of\ the\ outflowed\ carbon\ (mol)}$$

The catalytic performance could also be identified by apparent activation energy (E_a), which was measured as follows [S1]:

$$\ln r = \frac{-E_a}{RT} + C \quad (1)$$

In equation (1), r represented the reaction rate ($mol \cdot s^{-1}$), T referred to the reaction temperatures, and C was a constant term.

$$r = \frac{F \times X_{toluene}}{W} \quad (2)$$

In equation (2), $X_{toluene}$ denoted the conversion of toluene, F indicated the feeding rate ($mol \cdot s^{-1}$), and W corresponded to the mass of catalyst. Therefore, the plot of lnr and 1000/T yielded the E_a value.

We performed a kinetic study of the catalysts. The specific toluene reaction rates

through the catalyst's specific surface area (R_s) and the catalyst's mass (R_m) were calculated required the following equation [1]:

$$R_S = \frac{F \times \eta_{toluene}}{S_{BET}}$$

$$R_m = \frac{F \times \eta_{toluene}}{W}$$

$$\eta_{toluene} = \log \frac{1}{1 - \frac{X_{toluene}}{100}}$$

Table S1 Survey of literature data on catalytic oxidation of VOCs.

Catalysts	T_{90} (°C)	Pt content (wt%)	VOCs	WHSV ($mL \cdot h^{-1} \cdot g^{-1}$)	Concentration of VOCs (ppm)	Ref.
$Pt_{NC}@CeO_2$	272	0.0075	Toluene	30000	3000	This work
Pt/CeTi-11	152	0.5	Benzene	15000	1000	[2]
Pt-CeO_2/BEA-P	60	0.07	Toluene	120000	35	[3]
Pt/CeO_2-r	144	1.05	Toluene	45000	500	[4]

Table S2 The H_2 consumption (H_2-TPR) of each catalyst.

Catalyst	H_2 consumption (mmol/g)	
	The first peak	The second peak
$Pt_{NC}@CeO_2$	0.41	0.47
$Pt_{NP}@CeO_2$	0.35	0.41
Pt_{NP}/CeO_2	0.37	0.36
$Pt_{NP}@CeO_2$-MOF	0.51	0.57

Table S3 Distribution of infrared absorption bands appearing during the oxidation of toluene over Pt_{NC}@CeO_2 catalyst at different times and temperatures.

Position/cm^{-1}	Assignment	Characteristic of
3800-3500	metal−OH vibration and water molecules coordinated to the surface metal cations	metal coordination
2929, 2834	asymmetric and symmetric C−H stretching vibrations of the CH_2 group	benzyl
2362, 2335	\	CO_2 species
1960, 1867, 1800	asymmetric and symmetric C=O stretching vibrations of cyclic anhydrides	maleic anhydride
1750-1720, 1646	C=O stretching vibration of aldehydes	benzaldehyde
1618, 1505, 1438	skeleton stretching vibrations	aromatic ring
~1540, ~1400	asymmetric and symmetric COO stretching vibrations of carboxylate group	benzoate
~1370, 1153-1105, ~1078, 1063	C−O stretching vibrations of alkoxide species	benzyl alcohol
1362, 1311, 1302	\	maleic anhydride
1350	symmetrical −COO− stretching vibration of acetate species	acetate
1291	CH_2 deformation vibration of benzyl (C_6H_5−CH_2)	benzyl
1255	C−H bending vibration in the plane	/
1224	C−O stretching vibration of phenolate (C_6H_5O−H)	phenolate
~1030	C−H stretching vibration in-plane bending vibration	aromatic ring

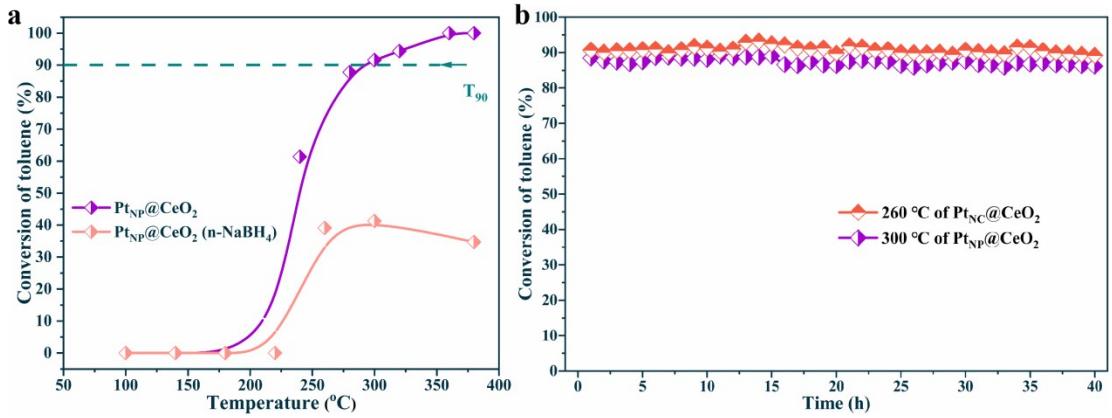

Fig. S1. The activity plot (a) of $Pt_{NP}@CeO_2$ and $Pt_{NP}@CeO_2$ (n-$NaBH_4$) catalysts. And the stability tests (b) of $Pt_{NC}@CeO_2$ and $Pt_{NP}@CeO_2$ at T_{90}.

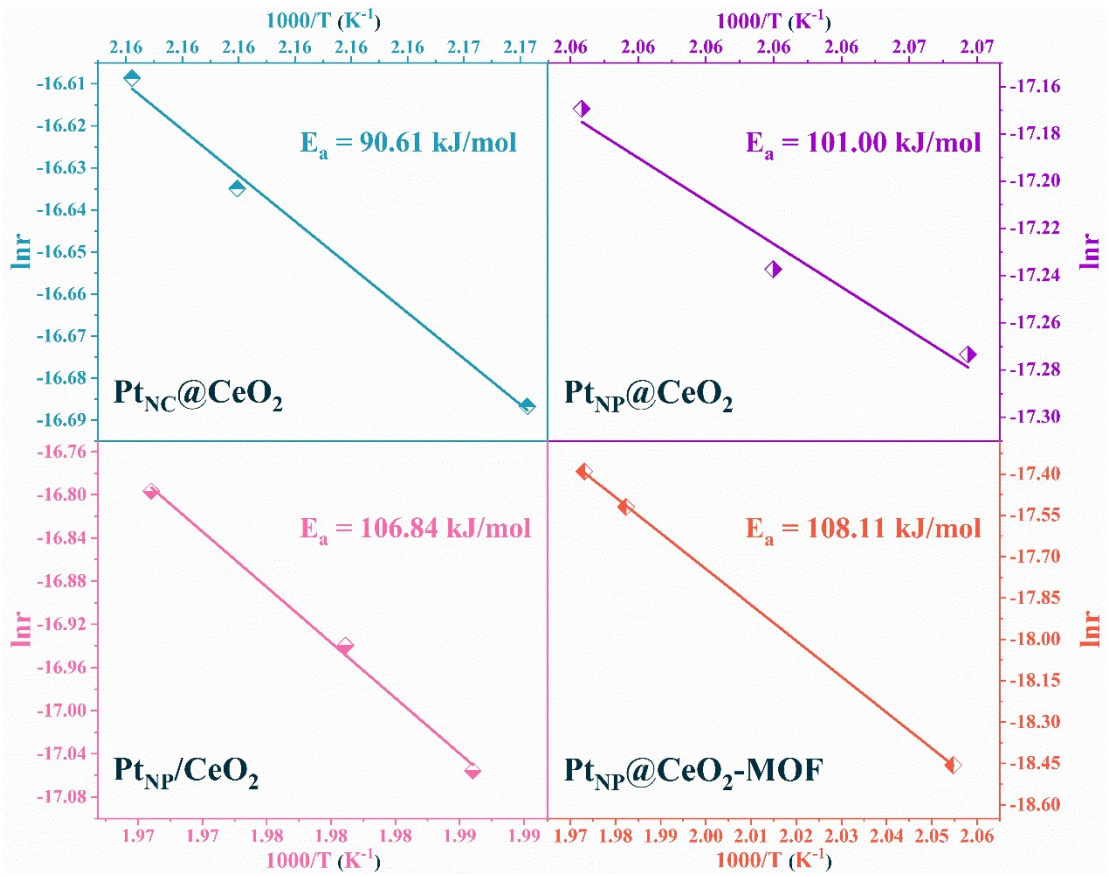

Fig. S2. The Arrhenius plot of four catalysts.

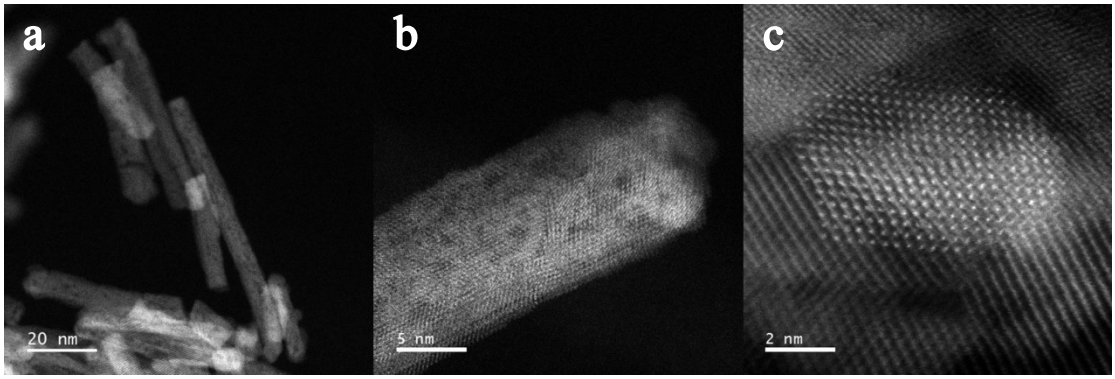

Fig. S3. HAADF-STEM images of the $Pt_{NP}@CeO_2$ catalyst.

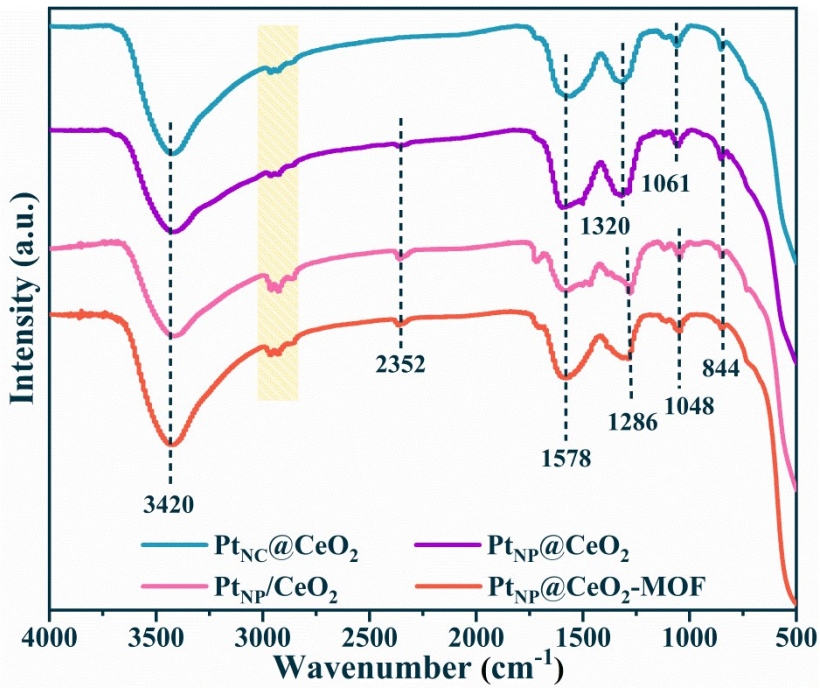

Fig. S4. FTIR spectrum of each catalyst.

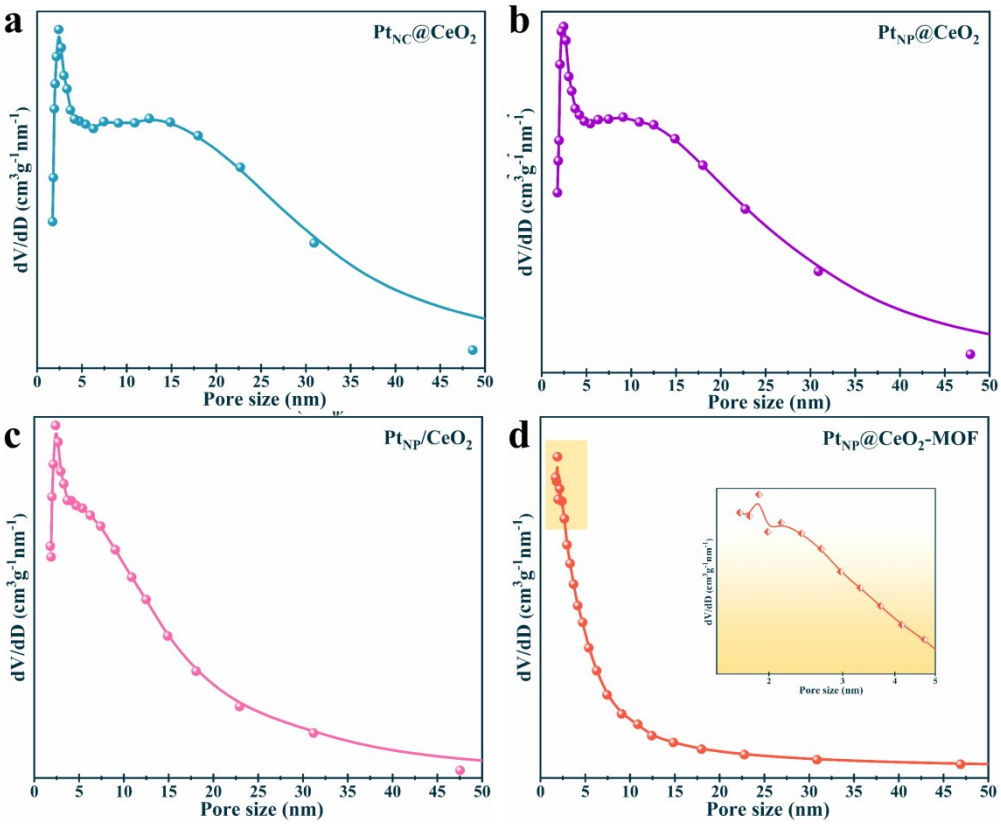

Fig. S5. The enlarged drawings about pore size distributions of $Pt_{NC}@CeO_2$ (a), $Pt_{NP}@CeO_2$ (b), Pt_{NP}/CeO_2-R (c), and $Pt_{NP}@CeO_2$-MOF (d).

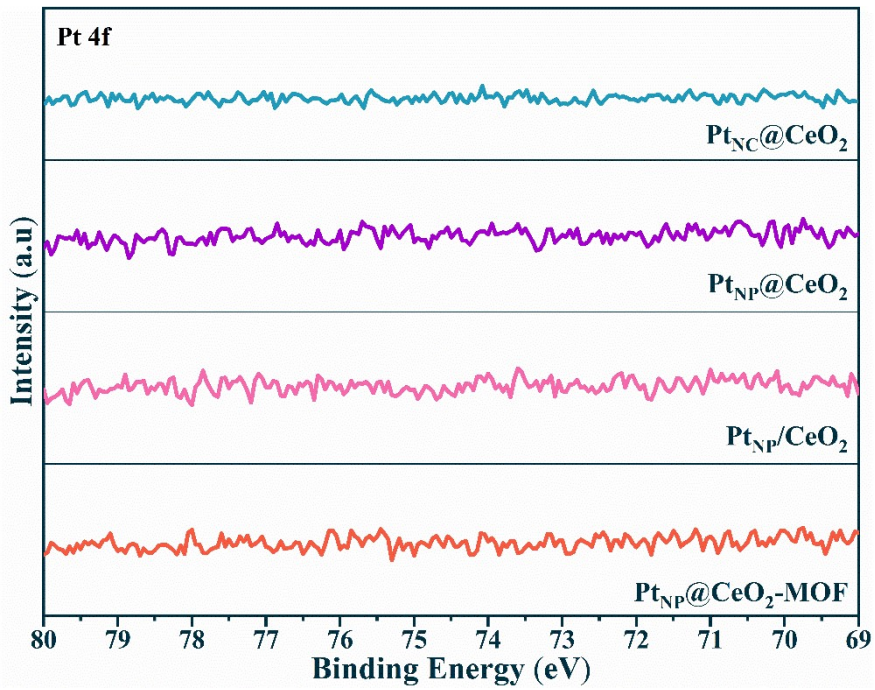

Fig. S6. The XPS spectra about Pt 4f of catalysts.

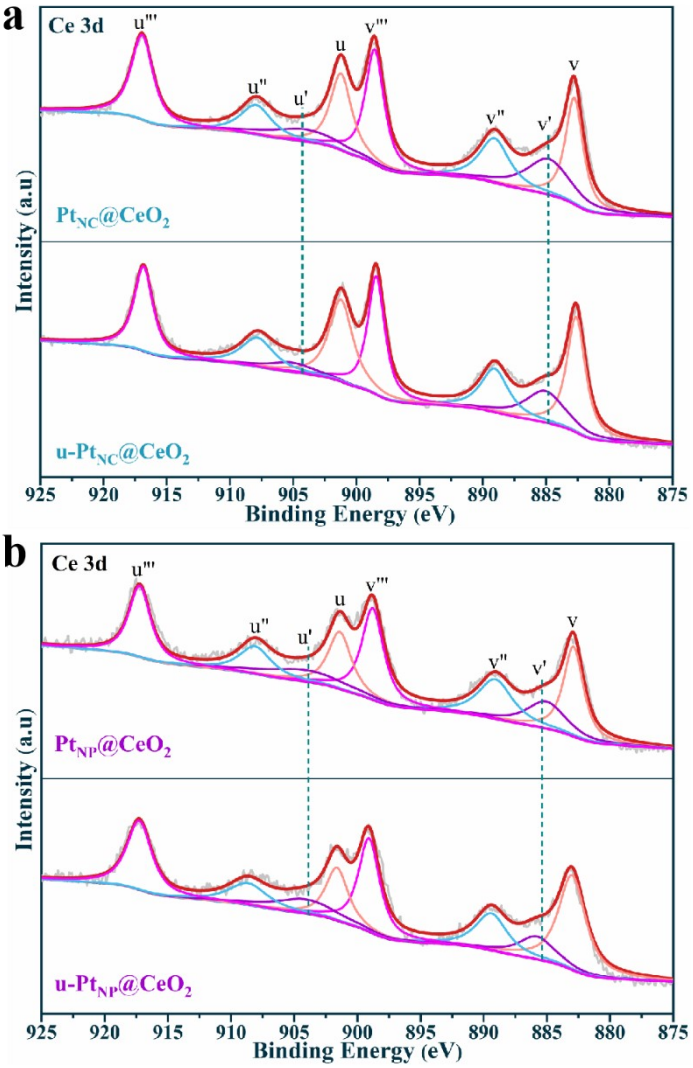

Fig. S7. The XPS spectra about Ce 3d of before and used comparison of $Pt_{NC}@CeO_2$ (a) and $Pt_{NP}@CeO_2$ (b) catalysts.

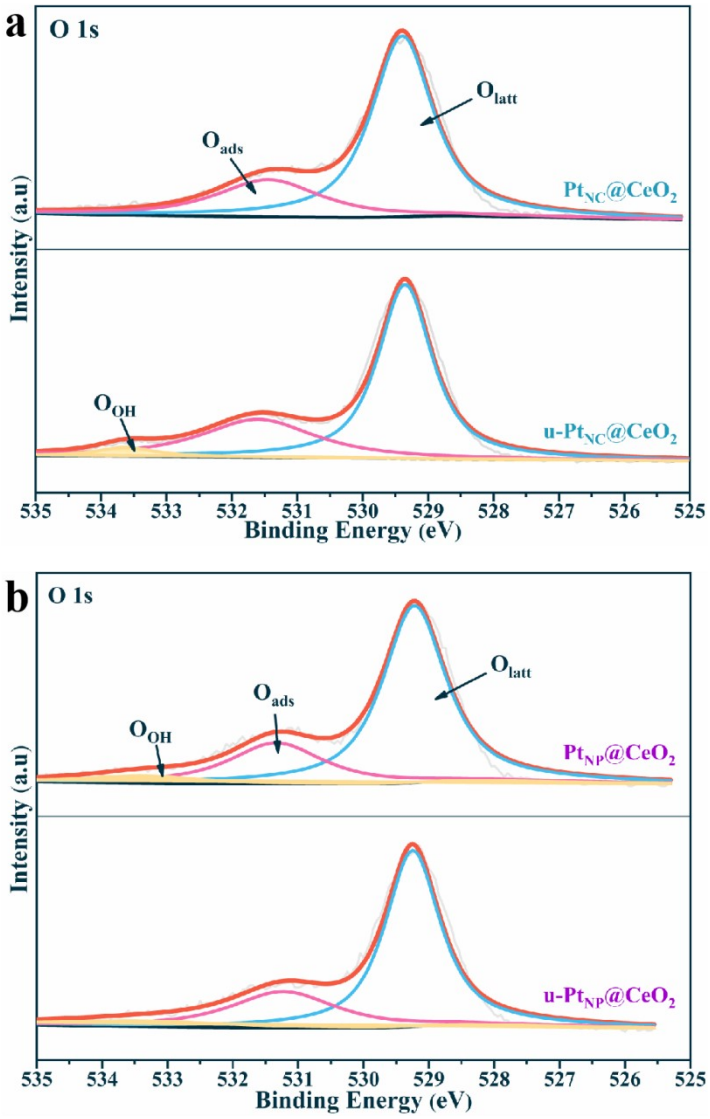

Fig. S8. The XPS spectra about O 1s of before and used comparison of $Pt_{NC}@CeO_2$ (a) and $Pt_{NP}@CeO_2$ (b) catalysts.

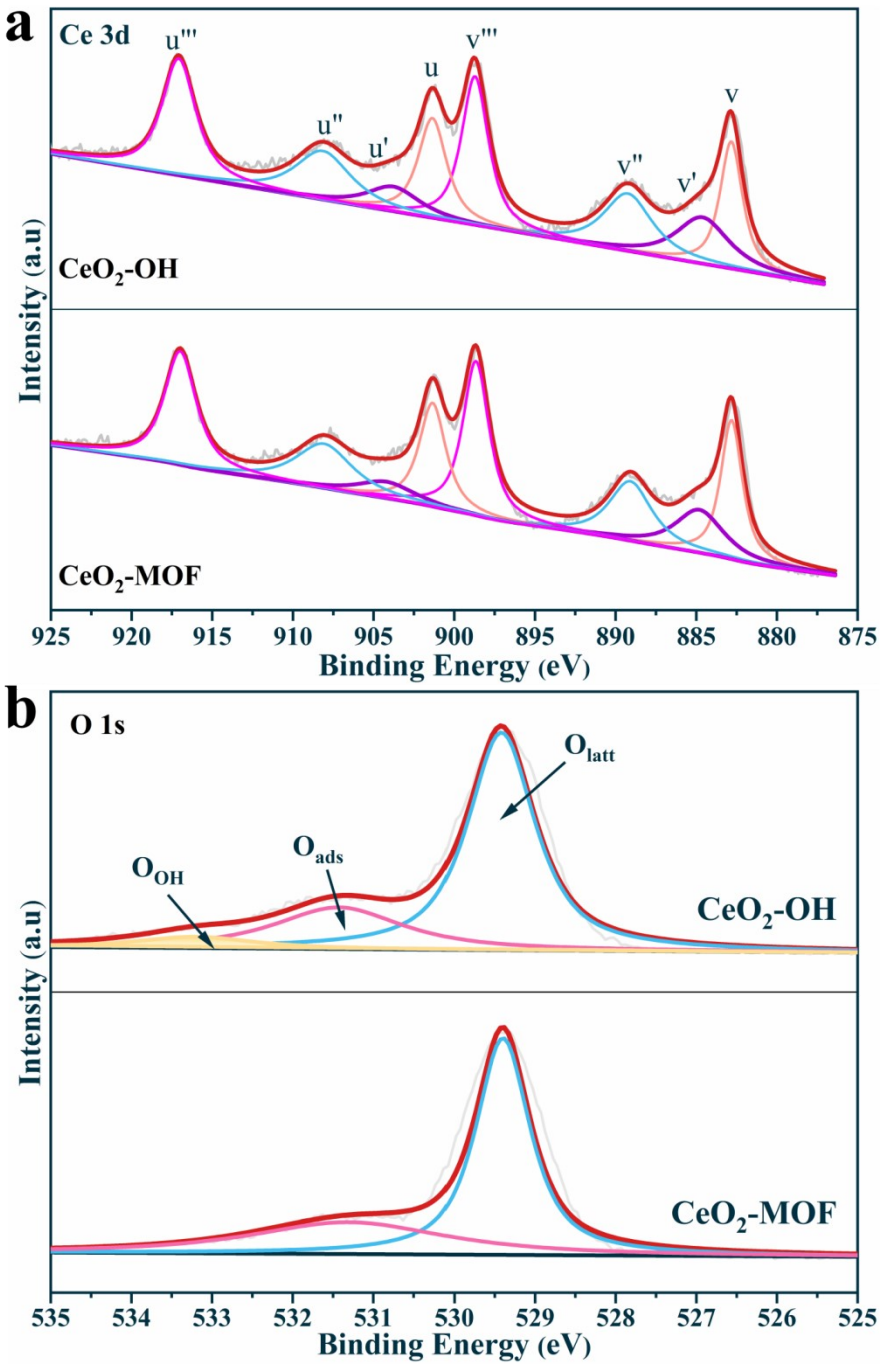

Fig. S9. The XPS spectra about Ce 3d (a) and O 1s (b) of CeO_2-OH and CeO_2-MOF catalysts.

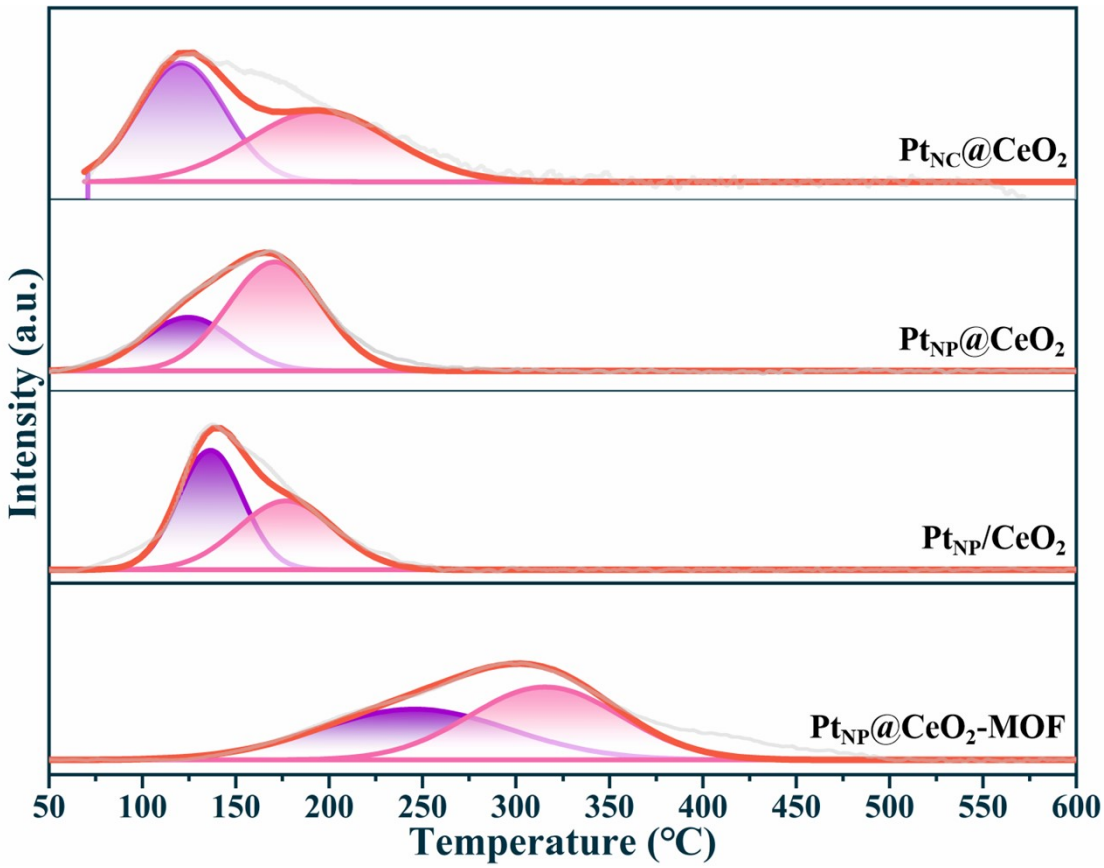

Fig. S10. H_2-TPR curves of the finely fitted peaks of the samples.

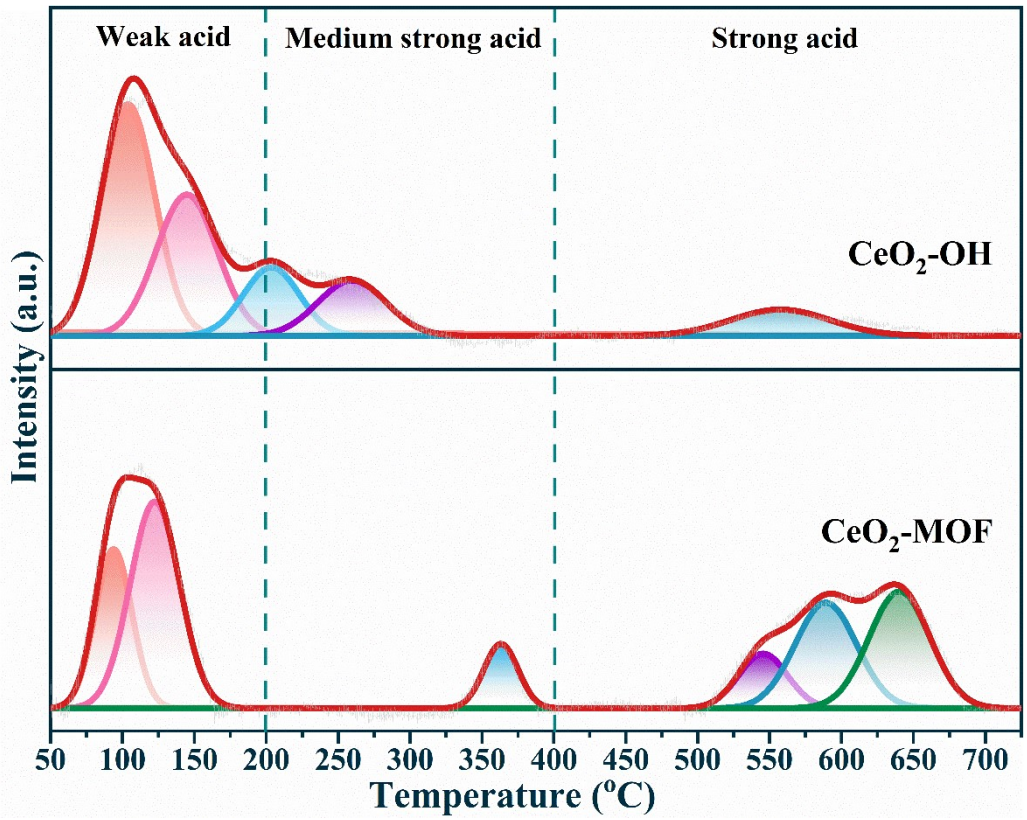

Fig. S11. NH_3-TPD profiles of CeO_2-OH and CeO_2-MOF samples.

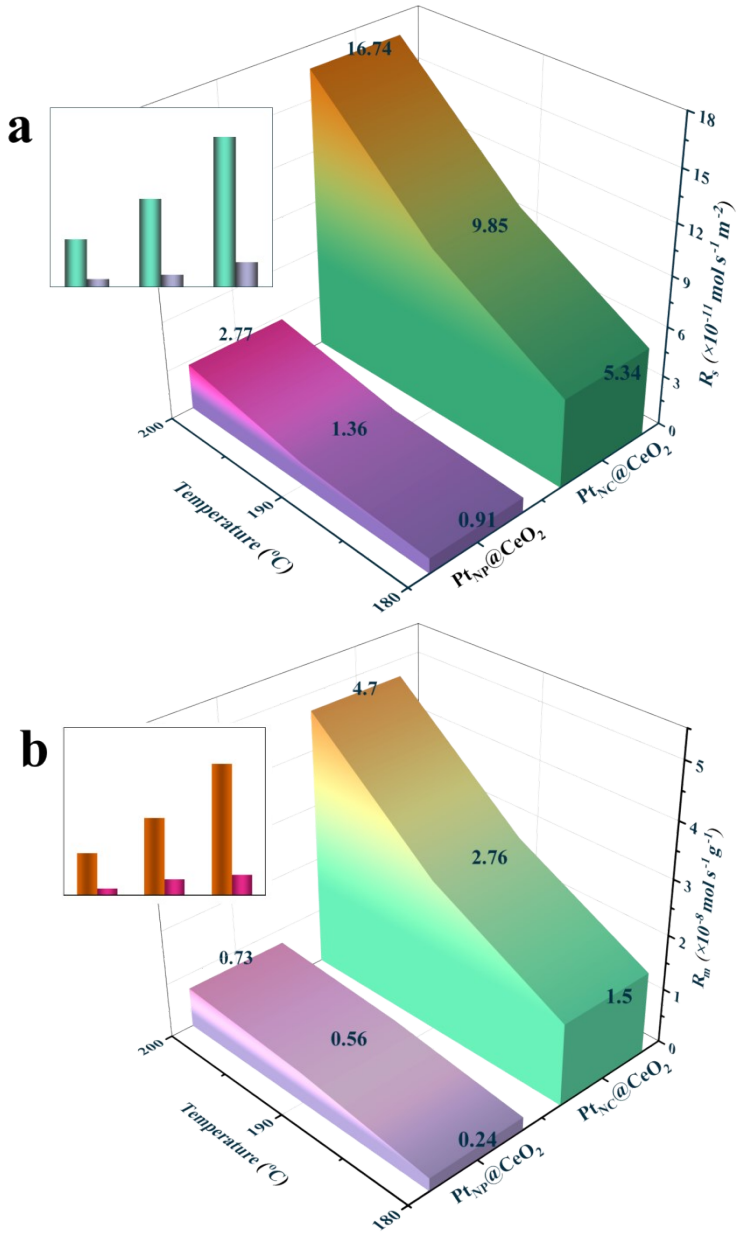

Fig. S12. Measurement of the specific toluene reaction rates of the Pt_{NC}@CeO_2 and Pt_{NP}@CeO_2 catalysts: R_s (a) and R_m (b).

References

[1] Q. Ren, S. Mo, R. Peng, Z. Feng, M. Zhang, L. Chen, M. Fu, J. Wu, D. Ye, Controllable synthesis of 3D hierarchical Co_3O_4 nanocatalysts with various morphologies for the catalytic oxidation of toluene, J. Mater. Chem. A, 6 (2018) 498-509.

[2] Y. Shi, J. Wang, R. Zhou, Pt-support interaction and nanoparticle size effect in Pt/CeO_2–TiO_2 catalysts for low temperature VOCs removal, Chemosphere, 265 (2021) 129127.

[3] J. Wang, X. Shi, L. Chen, H. Li, M. Mao, G. Zhang, H. Yi, M. Fu, D. Ye, J. Wu, Enhanced performance of low Pt loading amount on Pt-CeO_2 catalysts prepared by adsorption method for catalytic ozonation of toluene, Appl. Catal. A: Gen., 625 (2021) 118342.

[4] S. Chang, Y. Jia, Y. Zeng, F. Qian, L. Guo, S. Wu, J. Lu, Y. Han, Effect of interaction between different CeO_2 plane and platinum nanoparticles on catalytic activity of Pt/CeO_2 in toluene oxidation, J. Rare Earth., 40 (2022) 1743-1750.